Parameters Compensation of Permanent Magnet Synchronous Motor in Flux-Weakening Region for Rail Transit

Zisui Zhang, *Member, IEEE*, Chenchen Wang, *Member, IEEE*, Minglei Zhou, *Member, IEEE*, and Xiaojie You

***Abstract*—This article proposes a dual-parameters compensation control method to improve the torque accuracy of permanent magnet synchronous motor (PMSM) in flux-weakening region for rail transit. For the sake of the feature that six-step operation is the essential operation of rail transit and switching frequency is very low, the proposed method works on the single q-axis current regulator-variable voltage angle (SQCR-VVA) flux-weakening control strategy for PMSM operation. Based on SQCR-VVA flux-weakening control, impact of inaccurate parameters is analyzed in seven different conditions, and inaccurate parameters (d-axis inductance, q-axis inductance and permanent magnet flux linkage) result in the errors on d-axis current response and d-axis feed forward voltage. In order to eliminate the impact of the three parameters at the same time, dual compensation regulators are applied to the proposed method. Error of q-axis inductance is identified by the d-axis voltage regulator. The whole impact of inaccurate d-axis inductance and permanent magnet flux linkage is eliminated by the d-axis current regulator. The proposed method is subsequently tested on PMSM and shows quite good performance on the improvement of torque accuracy.**

***Index Terms*—Flux-weakening Control, PMSM, parameter compensation, torque accuracy.**

I. Introduction

USING permanent magnet synchronous motors (PMSMs) in rail transit system has attracted considerable attention in recent years [1]. PMSMs normally operate over a wide range of speed in locomotive and vehicles. It's an important issue that the torque controlled by flux-weakening method in high speed range should be accurate [2], [3]. However, torque command from superior control unit is converted to currents command with preset PMSM parameters, and actual torque is affected by actual PMSM parameters under controlled current(s). Without torque-closed loop control or speed-closed loop control, whether the torque is accurate depends on the errors between preset and actual PMSM parameters.

Manuscript received August 12, 2019; revised October 29, 2019, January 9, 2020, February 26, 2020, and March 24, 2020; accepted April 7, 2020. Date of publication April 12, 2020; date of current version July 20, 2020. This work was supported by the National Natural Science Foundation of China under Grant 51977006. Recommended for publication by Associate Editor K. Akatsu. *(Corresponding author: Chenchen Wang.)*

The authors are with the Beijing Jiaotong University, Beijing 100044, China (e-mail: 13117385@bjtu.edu.cn; chchwang@bjtu.edu.cn; zhouml@bjtu.edu.cn; xjyou@bjtu.edu.cn).

Color versions of one or more of the figures in this article are available online at https://ieeexplore.ieee.org.

Digital Object Identifier 10.1109/TPEL.2020.2987030

In order to improve the precision of torque, lots of parameter identification methods or flux observation methods are studied, such as look-up table (LUT) methods [4]–[6], recursive least square (RLS) methods [7]–[9], based on disturbance signal methods [10]–[13], model reference adaptive system (MRAS) methods [14]–[17], extended Kalman filter (EKF) methods [18], [19] and flux observation methods [20]–[22].

LUT methods are off-line parameter identification methods. Based on specific parameter, special experimental tests and proper measurement procedure should be carried out [4]. The off-line identified parameter may be limited to one parameter, such as permanent magnet flux linkage [5]. When more parameters are identified, more parameter maps and data storage space are needed [6]. Furthermore, the parameter maps based on LUT methods from one PMSM cannot be used perfectly to another type of PMSM in the rail transit. RLS methods can be designed as on-line parameter identification methods, which can avoid the problem when LUT methods are applied to different PMSMs. However, signal injection, which is not suitable to implement in rail transit, is a key to the RLS methods [7]–[9]. In rail transit drive system, PMSM mainly operates in square-wave mode when flux-weakening control is applied. For the square-wave mode, modulation strategy is in six-step operation and the output voltage magnitude is fixed as the maximum value. No injection disturbance signal can be added to the voltage command, so injection disturbance signal methods cannot be implemented in principle. Disturbance signals contain certain parameter information: rotor flux linkage can be estimated from distorted voltage due to inverter non-linearity in d-q reference frame [10], [12]; permanent magnet flux linkage can be estimated by using measured speed harmonics [11], [13]. To estimate flux linkage in rail transit, modulation of square wave mode reduces the number of deadband zone to two for each fundamental period and the impact of dead time can hardly be separated from the impact of voltage harmonics in square wave pluses. For rail transit, the speed harmonics may affected by different factors and the estimated permanent magnet flux linkage would be wrong. Additionally, inductance estimation is not mentioned in based on disturbance signal methods. Although MRAS, EKF and flux observation methods can be applied to identify parameters in rail transit, there are two difficulties caused by the PMSM mathematical model and low switching frequency. The first problem is that there are three parameters that affect the control of accuracy torque while only one or two of the parameters

can be identified [15], [16], [18], [19]. The second problem is that harmonic components of voltage reconstruction loop and current sampling loop in rail transit drive system can result in the wrong or bad response of the parameter identification methods. Accurate instantaneous d-axis, q-axis voltages and d-axis, q-axis currents are the guarantee of the accuracy of the identification algorithm. The observers in these on-line identification controls are based on the PMSM fundamental model and typically operate at a switching frequency of 2 kHz or even a switching frequency above 10 kHz [14], [17], [20]–[22]. When the corresponding filters are designed for elimination of the voltage/current harmonics in low switching frequency operation, the computational burden and control complexity of the control system will increase.

The ultimate goal of motor parameter identification is to improve torque accuracy. For the accurate torque control of rail transit system, an on-line parameter compensation method that is less affected by square wave conditions should be proposed. From the perspective of the current locus, the change of the motor parameters will result in the movement of actual current operating point. The command current operating point that is obtained from the uncompensated parameters is not located in the right position. When current regulators are applied, the actual current operating point is controlled at the wrong position. However, no current regulator is applied in variable voltage angle (VVA) flux-weakening control method. When the motor parameters change, there is an error between the current command operating point and the actual one. If d-axis or q-axis current regulator is introduced in VVA flux-weakening control method, the impact of inaccurate parameters will only affect the other axis current response.

In this article, a dual-parameter (q-axis inductance L_q, and d-axis flux ψ_d) compensation method for flux-weakening control is proposed. Based on the single q-axis current regulator-variable voltage angle (SQCR-VVA) flux-weakening control, the impact of three inaccurate parameters is analyzed in Section II firstly. Base on Section III, three PMSM parameters (permanent magnet flux linkage, d-axis inductance and q-axis inductance) that should be compensated can be reduced to two compensated parameters (d-axis inductance L_q and d-axis flux linkage ψ_d). Dual compensation regulators are designed base on the errors of d-axis current and d-axis voltage for the two compensated parameters. In Section IV, simulations and experiments are carried out to prove the effectiveness of the proposed method.

II. Impact of Inaccurate Parameters

A. Mathematical Model of PMSM

In synchronous dq-axes frame with synchronous angular speed ω_s, the voltage equations of a PMSM in the time domain are expressed as

$$\begin{aligned} u_d &= R_s i_d + sL_d i_d - \omega_s L_q i_q \\ u_q &= R_s i_q + sL_q i_q + \omega_s L_d i_d + \omega_s \psi_f \end{aligned} \tag{1}$$

where R_s is the stator resistance; u_d and u_q are the d-axis and q-axis stator voltages, respectively; i_d and i_q are the d-axis and q-axis stator currents, respectively; L_d and L_q are the d-axis and q-axis stator inductances, respectively; ω_s is the synchronous electromagnetic machine speed; ψ_f is the permanent magnet flux linkage; and s is the differential operator.

The torque equation can be expressed with three PMSM parameters as

$$T_e = \frac{3}{2} N_p \left(\psi_f + (L_d - L_q)\, i_d\right) i_q \tag{2}$$

where T_e is the electromagnetic torque; and N_p is the number of pole pairs.

Generally, the impact of L_d, L_q, and ψ_f on torque accuracy should be approached.

Voltage-fed inverters, are widely used in PMSM drive system. The inverter maximal phase voltage limit $u_{\max}$ is defined by the dc-link voltage u_{dc}, and $u_{\max}$ is $2u_{\text{dc}}/\pi$ for the rail transit system when PMSM operates in six-step operation, whereas the current limit $i_{\max}$ is defined by the machine rated current I_{rate} where the following must be fulfilled:

$$u_d^2 + u_q^2 = u_s^2 \le u_{\max}^2 \tag{3}$$

$$i_d^2 + i_q^2 = i_s^2 \le i_{\max}^2 = \left(\sqrt{2} I_{\text{rate}}\right)^2 \tag{4}$$

where u_s is the stator voltage vector magnitude; and i_s is the stator current magnitude.

For the speeds under the base speed, the dq-axes components of the current vector for the maximum torque-per-ampere (MTPA) are derived from (2) and (4) as follows:

$$i_d^2 + \frac{\psi_f}{L_d - L_q} i_d - i_q^2 = 0. \tag{5}$$

For the speeds above the base speed, neglecting the stator resistance, (1) can be simplified as

$$u_d = -\omega_s L_q i_q \tag{6}$$

$$u_q = \omega_s L_d i_d + \omega_s \psi_f. \tag{7}$$

When the speed is larger than the base speed in rail transit system, the PMSM is under flux-weakening control and in square-wave modulation mode. The voltage magnitude is fixed and only the voltage angle θ can be regulated. Then, (6) and (7) can be rewritten as

$$u_d = u_{\max} \cos\theta \tag{8}$$

$$u_q = u_{\max} \sin\theta. \tag{9}$$

B. SQCR-VVA Flux-Weakening Control

For the flux-weakening control of PMSM in six-step operation (SSO), the single q-axis current regulator variable voltage angle control method is applied with the feature that only q-axis current is used for the flux-weakening control [23]. The diagram of SQCR-VVA flux-weakening control method is shown in Fig. 1. There are two parts in the scheme: PART 1 is the command current loop, and PART 2 is the single q-axis current regulator loop.

In SQCR-VVA flux-weakening control scheme, q-axis current is controlled by the single q-axis regulator while no regulator is designed to control d-axis current. No matter how the

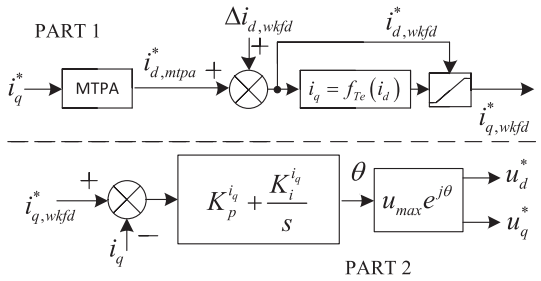

Fig. 1. Diagram of SQCR-VVA flux-weakening control method.

parameters change, actual q-axis current in the SQCR-VVA flux-weakening control scheme normally controlled as

$$i_q^* = i_q^m \tag{10}$$

where i_q^* is the command q-axis current and i_q^m is the actual q-axis current.

When the parameters are accurate, the actual d-axis current and torque are also the same as their command values.

C. Errors on d-Axis Current and d-Axis Voltage

Actual d-axis current may not equal its command value under the inaccurate parameters conditions, because there is no d-axis current regulator to track the d-axis command current. Meanwhile, there may be also an error between the actual torque and its command value due to the impact of inaccurate parameters. The errors should be analyzed. In order to analysis the impact of inaccurate parameters, there are two groups of PMSM parameters: the parameters used in the control algorithm (L_d, L_q, and ψ_f), and the actual parameters ($\hat{L}_d$, $\hat{L}_q$, and $\hat{\psi}_f$). The two groups of PMSM parameters can be expressed as

$$\hat{L}_d = (1+\alpha) L_d \tag{11}$$

$$\hat{L}_q = (1+\beta) L_q \tag{12}$$

$$\hat{\psi}_f = (1+\gamma) \psi_f. \tag{13}$$

In order to simplify the variable parameters conditions, PMSM parameter variation range can be generally set as

$$\begin{aligned} -0.6 \le \alpha \le 0.6 \\ -0.4 \le \beta \le 0.4 \\ -0.2 \le \gamma \le 0.2 \end{aligned} \tag{14}$$

where α is the coefficient of variation of L_d; β is the coefficient of variation of L_q; γ is the coefficient of variation of ψ_f; $\beta > \rho\alpha$, $\rho = L_q/L_d$; and they all are decimal.

For the sake that permanent magnet materials are buried in the rotor for interior permanent magnet synchronous motor (IPMSM), q-axis inductance is always larger than the d-axis inductance under changed motor parameters condition, and the polarity characteristics of the IPMSM normally cannot change. Then the following relationship between α and β should be satisfied to keep the property of $\hat{L}_q < \hat{L}_d$.

$$(1+\beta) L_q \ge (1+\alpha) L_d. \tag{15}$$

For the whole control system, there are three groups of d/q voltages: the forward feedback d/q voltages (u_d^{fw} and u_q^{fw}), the command d/q voltages (u_d^* and u_q^*), and the actual d/q voltages (u_d^m and u_q^m). In the flux-weakening control, the voltage drops on IGBT can be neglected. For the actual d-axis current response calculation with inaccurate parameters, u_d^{fw} and u_q^{fw} are calculated with L_d, L_q, and ψ_f.

The actual d/q voltages should be the same as the command d/q voltage:

$$u_d^m = u_d^* \tag{16}$$

$$u_q^m = u_q^*. \tag{17}$$

In the flux-weakening region, the voltage magnitude is fixed as $u_{\max}$:

$$\left(u_d^{\mathrm{fw}}\right)^2 + \left(u_q^{\mathrm{fw}}\right)^2 = (u_d^*)^2 + \left(u_q^*\right)^2 = (u_d^m)^2 + \left(u_q^m\right)^2 = u_{\max}^2. \tag{18}$$

Based on (6), (10), (11)–(13), and (16), u_d^* can be expressed by u_d^{fw} and β.

$$\begin{aligned} i_q^* &= i_q^m \\ -\omega_s L_q i_q^* &= -\omega_s L_q i_q^m \\ (1+\beta)\, u_d^{\mathrm{fw}} &= -\omega_s (1+\beta) L_q i_q^m \\ (1+\beta)\, u_d^{\mathrm{fw}} &= -\omega_s \hat{L}_q i_q^m \\ (1+\beta)\, u_d^{\mathrm{fw}} &= u_d^m = u_d^* \\ u_d^m &= (1+\beta)\, u_d^{\mathrm{fw}}. \end{aligned} \tag{19}$$

Based on (7), (11)–(13), and (16)–(19), the actual d-axis under inaccurate parameters can be calculated with inaccurate parameters

$$\begin{aligned} (u_d^m)^2 + \left(u_q^m\right)^2 &= u_{\max}^2 \\ \left(u_q^m\right)^2 &= u_{\max}^2 - (u_d^m)^2 \\ \left(u_q^m\right)^2 &= u_{\max}^2 - (u_d^*)^2 \\ \left(u_q^m\right)^2 &= u_{\max}^2 - (1+\beta)^2 \left(u_d^{\mathrm{fw}}\right)^2 \\ \left(u_q^m\right)^2 &= u_{\max}^2 - (1+\beta)^2 \left(u_{\max}^2 - \left(u_q^{\mathrm{fw}}\right)^2\right) \\ \left(\hat{L}_d i_d^m + \hat{\psi}_f\right)^2 &= (1+\beta)^2 (L_d i_d^* + \psi_f)^2 - \left(2\beta+\beta^2\right) \frac{u_{\max}^2}{\omega_s^2} \end{aligned}$$

$$i_d^m = \frac{-(1+\gamma)\psi_f + \sqrt{(1+\beta)^2 (L_d i_d^* + \psi_f)^2 - (2\beta+\beta^2) \frac{u_{\max}^2}{\omega_s^2}}}{(1+\alpha) L_d}. \tag{20}$$

Equation (20) can be simply rewritten as

$$i_d^m = f(i_d^*, \alpha, \beta, \gamma). \tag{21}$$

There is also an error between the actual torque and the command torque. The expression of the actual torque is very complicated due to the complicated actual d-axis current, so the impact of inaccurate parameters on actual torque will be

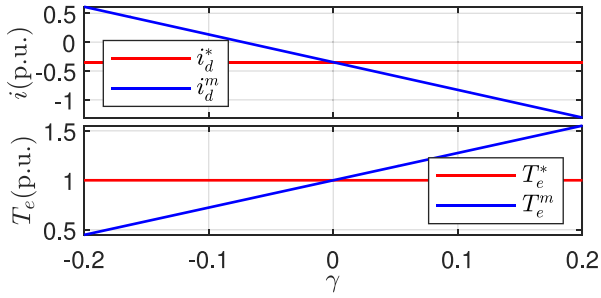

Fig. 2. Actual i_d^m and T_e^m response with $\hat{\psi}_f$.

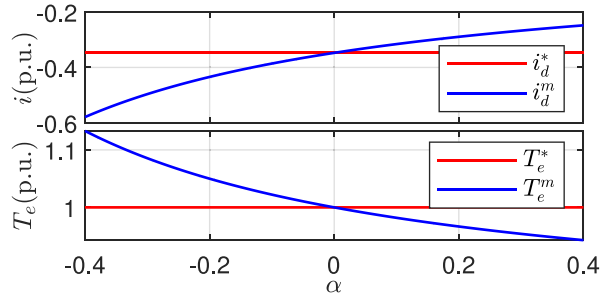

Fig. 3. Actual i_d^m and T_e^m response with $\hat{L}_d$.

analysed in different cases with figures and necessary equations in next section.

Although i_d^* can be regarded as a constant, the relationship between the axis current command and the actual value should be explained in a four-dimensional diagram. It is impossible to visually display the four-dimensional graphics in two-dimensional space. The characteristics of i_d can be discussed by assuming that some of the parameters are unchanged.

III. Proposed Parameter Compensation Control Scheme

Torque accuracy is affected by three PMSM parameters in (2), namely L_d, L_q and ψ_f. Based on (21), parameter compensation methods are designed for seven different inaccurate parameters conditions in this section. For a general parameters compensation, compensation of L_d, L_q, and ψ_f are substituted by compensation of L_q and ψ_d through q-axis inductance compensation coefficient $\beta_{\rm cmp}$ and d-axis flux compensation value $\Delta\psi_d^{\rm cmp}$.

A. Compensation of Single Inaccurate Parameter

When single parameter is inaccurate, there are three cases in total.

1) $\hat{\psi}_f$: When only permanent magnet flux linkage is inaccurate, (19) can be simplified as (22) and actual torque is calculated by (23).

$$i_d^m = i_d^* - \frac{\psi_f}{L_d}\gamma \tag{22}$$

$$T_e^m = T_e^* + \frac{3}{2}N_p\frac{L_q}{L_d}\gamma\psi_f i_q^* \tag{23}$$

where T_e^* and T_e^m are the command and actual torque, respectively.

The impact of γ on the actual d-axis current and torque is $-\psi_f\gamma/L_d$ and $3N_pL_q\psi_f i_q^*\gamma/2L_d$, which can be illustrated by Fig. 2. Only when $\hat{\psi}_f$ is accurate ($\gamma = 0$), the actual values of i_d and T_e are equal to their command values, respectively. When $\hat{\psi}_f$ is inaccurate ($\gamma \neq 0$), i_d^m and T_e^m are not equal to the command values.

The direct compensation $\gamma^{\rm cmp}$ can be set from (22):

$$\gamma^{\rm cmp} = \frac{L_d}{\psi_f}\left(i_d^* - i_d^m\right). \tag{24}$$

2) $\hat{L}_d$: When only d-axis inductance is inaccurate, i_d^m and T_e^m can be calculated as

$$i_d^m = \frac{1}{1+\alpha}i_d^* \tag{25}$$

$$T_e^m = T_e^* + \frac{3}{2}N_p\frac{1}{1+\alpha}L_q i_d^* i_q^*. \tag{26}$$

The impact of α on the actual d-axis current and torque is $i_d^*/(1+\alpha)$ and $3N_pL_q i_d^* i_q^*/(1+\alpha)$, which can be illustrated by Fig. 3. Only when $\hat{L}_d$ is accurate ($\alpha = 0$), the actual values of i_d and T_e are equal to their command values, respectively. When $\hat{L}_d$ is inaccurate ($\alpha \neq 0$), i_d^m and T_e^m are not equal to the command values.

The direct compensation $\alpha^{\rm cmp}$ can be set from (25):

$$\alpha^{\rm cmp} = \frac{i_d*}{i_d^m} - 1. \tag{27}$$

However, the actual i_d^m appears in the denominator in (27). When PMSM operates in low-load operation or zero-load, the zero or small value of i_d^m will result in the wrong compensation from (27). The indirectly compensation $\alpha^{\rm cmp}$ of L_d can be improved from the d-axis current regulator:

$$\alpha^{\rm cmp} = -\frac{K_i^{id} + sK_p^{id}}{s}\left(i_d^* - i_d^m\right) \tag{28}$$

where K_p^{id} and K_i^{id} are the proportional coefficient and integral coefficient, respectively. $K_p^{id} > 0$ and $K_i^{id} > 0$.

3) $\hat{L}_q$: When only q-axis inductance is inaccurate, i_d^m can be calculated as

$$i_d^m = \frac{-\psi_f - \sqrt{(1+\beta)^2\left(L_d i_d^* + \psi_f\right)^2 - (2\beta+\beta^2)\frac{u_{\max}^2}{\omega_s^2}}}{L_d}. \tag{29}$$

Equation (29) can be transformed as a quadratic equation

$$A\beta^2 + 2A\beta + C = 0 \tag{30}$$

where $A = \omega_s(L_d i_d^* + \psi_f)^2 - u_{\max}^2$
$C = \omega_s^2((L_d i_d^* + \psi_f)^2 - (L_d i_d^m + \psi_f)^2)$.

Since the expression of i_d is complicated, the equation of T_e is not expressed. The impact of β on the actual d-axis current and torque is directly illustrated by Fig. 4. Only when $\hat{L}_q$ is accurate ($\beta = 0$), the actual values of i_d and T_e are equal to their command values, respectively. When $\hat{L}_q$ is inaccurate ($\beta \neq 0$),

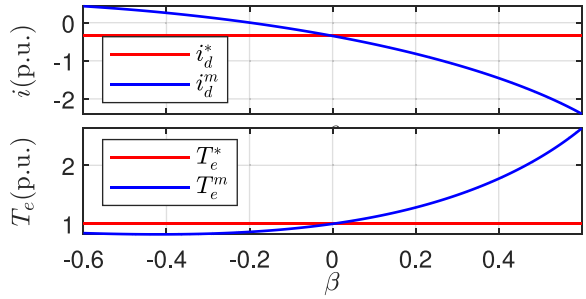

Fig. 4. Actual i_d^m and T_e^m response with $\hat{L}_q$.

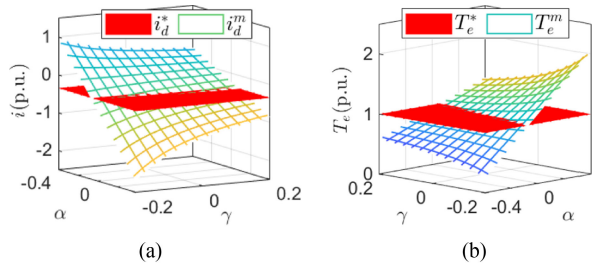

Fig. 5. Actual i_d^m and T_e^m response with $\hat{\psi}_f$ and $\hat{L}_d$: (a) i_d^m; (b) T_e^m.

i_d^m and T_e^m are not equal to the command values. The symmetry axis of (30) is $\beta = -1$. Since L_q is always greater than zero, actual β is also always greater than -1. For the variation of β in $[-0.4, 0.4]$, the impact of β is monotonous.

The direct compensation β^{cmp} can be realized by the root of the quadratic equation in (30):

$$\beta^{\text{cmp}} = -1 + \frac{\sqrt{A^2 - AC}}{A}. \tag{31}$$

Although (31) gives a clear solution, the direct compensation calculation process is complicated. In order to simplify the compensation, another direct compensation β^{cmp} can be obtained by (20)

$$\beta^{\text{cmp}} = \frac{u_d^*}{u_d^{\text{fw}}} - 1. \tag{32}$$

There is the same problem of (27) and (32), and then, the indirect compensation β^{cmp} of L_q can be improved from the d-axis current regulator:

$$\beta^{\text{cmp}} = \frac{K_i^{i_d} + sK_p^{i_d}}{s}\left(i_d^* - i_d^m\right) \tag{33}$$

where $K_p^{i_d}$ and $K_i^{i_d}$ are the proportional coefficient and integral coefficient, respectively. $K_p^{i_d} > 0$ and $K_i^{i_d} > 0$.

For the single inaccurate parameter, the conclusion is that when the error between i_d^* and i_d is regulated to zero, the inaccurate parameter is compensated and the output torque is corrected.

B. Compensation of Two Inaccurate Parameters

When two parameters are inaccurate, there are also three cases in total.

1) $\hat{\psi}_f$ and $\hat{L}_d$: When both permanent magnet flux linkage and d-axis inductance are inaccurate, i_d^m can be simplified as

$$i_d^m = \frac{L_d i_d^* - \psi_f \gamma}{(1+\alpha)L_d}. \tag{34}$$

The impact of both α and γ on the actual d-axis current and torque is directly illustrated by Fig. 5. When $\hat{L}_d$ and $\hat{\psi}_f$ are accurate ($\alpha = 0$ and $\gamma = 0$), the actual values of i_d and T_e are equal to their command values, respectively.

The actual d-axis current plane intersects the command d-axis current plane in a straight line. When α and γ are not zero but on this line, the actual d-axis and torque are the same as their command values, respectively. This special line is

$$L_d i_d^* \alpha + \psi_f \gamma = 0. \tag{35}$$

The error of d-axis current is also can be used to compensate the inaccurate parameters. However, the design of compensation encounters the deficiency-rank problem. α and γ can not be compensated separately at the same time with the only error of d-axis current. In order to realize the compensation of the impact of the two parameters, a new parameter that is influenced by the two parameters should be found. Considering that ψ_f and L_d are both in (2), the new form of (2) can be expressed as

$$T_e = \frac{3}{2} N_p \left(\psi_d - L_q i_d\right) i_q \tag{36}$$

where $\psi_d = L_d i_d + \psi_f$

Based on (36), the impact of α and γ is equivalent to the impact of ψ_d. When ψ_d is compensated by error of d-axis current, the actual torque can be accurate. The indirect compensation $\Delta\psi_d^{\text{cmp}}$ is

$$\Delta\psi_d^{\text{cmp}} = \frac{K_i^{i_d} + sK_p^{i_d}}{s}\left(i_d^* - i_d^m\right) \tag{37}$$

where $K_p^{i_d}$ and $K_i^{i_d}$ are the proportional coefficient and integral coefficient, respectively. $K_p^{i_d} > 0$ and $K_i^{i_d} > 0$.

Furthermore, the compensation method with ψ_d is suitable for the compensation of single L_d and ψ_f in condition A.1) and A.2), respectively. The improvement of torque accuracy is the ultimate control object. It is not required that all the inaccurate parameters should be accurate to perform torque estimation or improve the accuracy of torque. When there are difficulties in compensation of all the inaccurate parameters at the same time, the improvement of torque accuracy can be achieved by the indirect parameter, such as ψ_d.

2) $\hat{L}_d$ and $\hat{L}_q$: When both d-axis and q-axis inductance are inaccurate, i_d^m can be simplified as

$$i_d^m = \frac{-\psi_f - \sqrt{(1+\beta)^2\left(L_d i_d^* + \psi_f\right)^2 - \left(2\beta + \beta^2\right)\frac{u_{\max}^2}{\omega_s^2}}}{(1+\alpha)L_d}. \tag{38}$$

The impact of both α and β on the actual d-axis current and torque is directly illustrated by Fig. 6. When $\hat{L}_d$ and $\hat{L}_q$ are accurate ($\alpha = 0$ and $\beta = 0$), the actual values of i_d and T_e are equal to their command values, respectively.

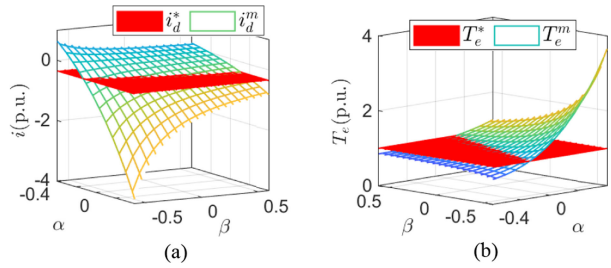

Fig. 6. Actual i_d^m and T_e^m response with $\hat{L}_d$ and $\hat{L}_q$: (a) i_d^m; (b) T_e^m.

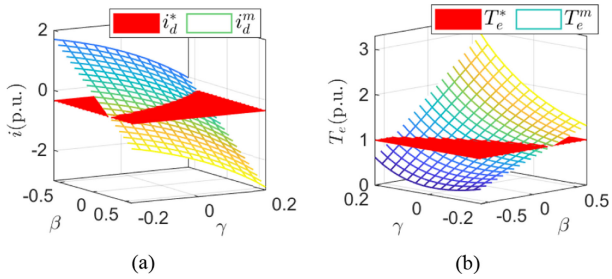

Fig. 7. Actual i_d^m and T_e^m response with $\hat{\psi}_f$ and $\hat{L}_q$: (a) i_d^m; (b) T_e^m.

The actual d-axis current plane intersects the command d-axis current plane in an elliptic curve which is

$$\frac{\left(\alpha+\frac{\psi_f+L_d i_d^*}{L_d i_d^*}\right)^2}{\left(\frac{u_{\max}}{\omega_s L_d i_d^*}\right)^2}+\frac{(\beta+1)^2}{\left(\frac{u_{\max}}{\omega_s L_q i_q^*}\right)^2}=1. \tag{39}$$

When α and β are satisfied by (39), the actual i_d is equal to its command value. When actual T_e is equal to its command value, α and β should be satisfied by a straight line limit:

$$L_d\alpha - L_q\beta = 0. \tag{40}$$

Based on the shape of a line and the shape of a ellipse, the curve of (39) and the curve of (40) do not coincide. This misalignment results in that when the d-axis current error is adjusted to 0 by the compensation of the d-axis current regulator, the actual torque is still not the same as its command value.

The error of i_d can not compensate the impact of α and β at the same time. There is no steady parameter that is formed by L_d and L_q. To solve the deficiency-rank problem, one solution is that two parameter is combined to form the new parameter, and another solution is that a new error is introduced to increase the rank. It's difficult to find a equation of first degree that is expressed by L_d and L_q at the same time. According to (20), β can be compensated by the error of u_d, the error between u_d^* and u_d^{fw}. When β is compensated, the inaccurate parameter problem is simplified as inaccurate L_d problem, and α can be compensated by the error of i_d. Then the indirect dual compensation regulators are expressed as

$$\begin{aligned}\alpha^{\text{cmp}} &= -\frac{K_i^{i_d}+sK_p^{i_d}}{s}\left(i_d^*-i_d^m\right)\\ \beta^{\text{cmp}} &= \frac{K_i^{u_d}+sK_p^{u_d}}{s}\left(u_d^{\text{fw}}-u_d^*\right)\end{aligned} \tag{41}$$

where $K_p^{i_d}>0$, $K_i^{i_d}>0$, $K_p^{u_d}>0$, and $K_i^{u_d}>0$.

3) $\hat{\psi}_f$ and $\hat{L}_q$: When both permanent magnet flux linkage and q-axis inductance are inaccurate, i_d^m can be simplified as

$$i_d^m=\frac{-(1+\gamma)\psi_f-\sqrt{(1+\beta)^2\left(L_d i_d^*+\psi_f\right)^2-(2\beta+\beta^2)\frac{u_{\max}^2}{\omega_s^2}}}{L_d}. \tag{42}$$

The impact of both β and γ on the actual d-axis current and torque is directly illustrated by Fig. 7. When $\hat{L}_q$ and $\hat{\psi}_f$ are accurate ($\beta=0$ and $\gamma=0$), the actual values of i_d and T_e are equal to their command values, respectively.

The actual d-axis current plane intersects the command d-axis current plane in an elliptic curve which is

$$\frac{\left(\gamma+\frac{L_d}{\psi_f}i_d^*+1\right)^2}{\left(\frac{u_{\max}}{\omega_s\psi_f}\right)^2}+\frac{(\beta+1)^2}{\left(\frac{u_{\max}}{\omega_s L_q i_q^*}\right)^2}=1. \tag{43}$$

When β and γ are satisfied by (43), the actual i_d is equal to its command value. When actual T_e is equal to its command value, β and γ should be satisfied by a straight line limit:

$$L_d\alpha - L_q\beta = 0. \tag{44}$$

Base on the shape of a line and the shape of a ellipse, the curve of (43) and the curve of (44) do not coincide. This misalignment results in that when the d-axis current error is adjusted to 0 by the compensation of the d-axis current regulator, the actual torque is still not the same as its command value.

It's difficult to find a equation of first degree that is expressed by L_q and ψ_f at the same time. According to (20), β can be compensated by the error of u_d, the error between u_d^* and u_d^{fw}. When β is compensated, the inaccurate parameter problem is simplified as inaccurate ψ_f problem, and γ can be compensated by the error of i_d. In the same way, γ can be compensated by the error of i_d, and β can be compensated by the error of u_d, the error between u_d^* and u_d^{fw}. Then the indirect dual compensation regulator are expressed as

$$\begin{aligned}\beta^{\text{cmp}} &= \frac{K_i^{u_d}+sK_p^{u_d}}{s}\left(u_d^{\text{fw}}-u_d^*\right)\\ \gamma^{\text{cmp}} &= \frac{K_i^{i_d}+sK_p^{i_d}}{s}\left(i_d^*-i_d^m\right)\end{aligned} \tag{45}$$

where $K_p^{i_d}>0$, $K_i^{i_d}>0$, $K_p^{u_d}>0$, and $K_i^{u_d}>0$.

For the two inaccurate parameters, the conclusion is that when the two parameter are in the same equation, only the error of i_d can be used to compensate; otherwise, the error of u_d should be introduced.

C. Compensation of Three Inaccurate Parameters

In this case, permanent magnet flux linkage, d-axis inductance and q-axis inductance are all inaccurate. According to the aforementioned compensations for the 6 different inaccurate parameters conditions, the error of i_d and u_d should be used at the same time when the three parameters are inaccurate. Finally,

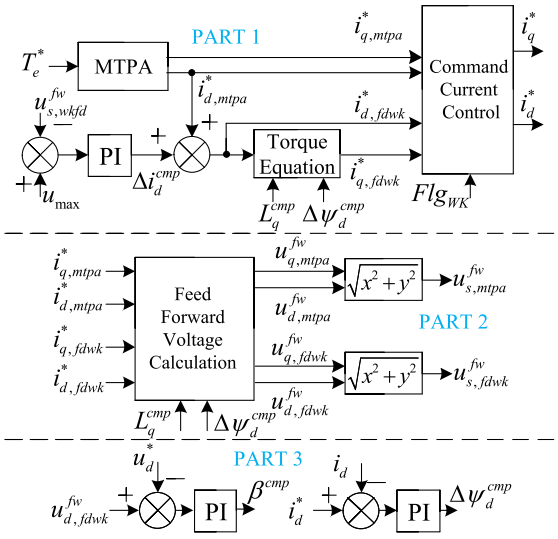

Fig. 8. Diagram of SQCR-VVA flux-weakening control with parameters compensation.

the indirect dual compensation regulators can be expressed as:

$$\begin{aligned}\beta^{\mathrm{cmp}} &= \frac{K_i^{u_d}+sK_p^{u_d}}{s}\left(u_d^{\mathrm{fw}}-u_d^*\right)\\ \Delta\psi_d^{\mathrm{cmp}} &= \frac{K_i^{i_d}+sK_p^{i_d}}{s}\left(i_d^*-i_d^m\right)\end{aligned} \tag{46}$$

where β^{cmp} is the compensation value of L_q, and $\Delta\psi_d^{\mathrm{cmp}}$ is the compensation value of ψ_d.

Based on SQCR-VVA flux-weakening control method, the diagram with parameters compensation is shown in Fig. 8. The variable with subscript s is the variable of magnitude. The variable with subscript d or q is the variable in d-axis or q-axis. The variable with subscripts $mtpa$ or $wkfd$ is the variable used in MTPA control or flux-weakening control. The variable with superscripts $*$, fw or cmp is the variable obtained from command loop, feed forward loop or compensation loop, respectively.

There are three parts in Fig. 8. PART 1 is the current command part of flux-weakening control method; PART 2 is the feed forward voltage calculation loop; and PART 3 is the parameters compensation loop.

For the torque equation in PART 1 in Fig. 8, (36) is improved as

$$i_{q,\mathrm{wkfd}}^* = \frac{2T_e^*}{3N_p\left(\psi_d^{\mathrm{cmp}}-L_q^{\mathrm{cmp}}i_{d,\mathrm{wkfd}}\right)}. \tag{47}$$

For the feed forward voltage calculation in PART 2 in Fig. 8, (6) and (7) are improved as

$$\begin{aligned}L_q^{\mathrm{cmp}} &= \left(1+\beta^{\mathrm{cmp}}\right)L_q\\ u_d^{\mathrm{fw}} &= -\omega_s L_q^{\mathrm{cmp}} i_q^*\\ u_q^{\mathrm{fw}} &= \omega_s L_d i_d^* + \omega_s\psi_f + \omega_s\Delta\psi_d^{\mathrm{cmp}}\end{aligned} \tag{48}$$

where $i_d^* = i_{d,\mathrm{mtpa}}^*$ and $i_q^* = i_{q,\mathrm{mtpa}}^*$ when MTPA control is applied; and $i_d^* = i_{d,\mathrm{wkfd}}^*$, and $i_q^* = i_{q,\mathrm{wkfd}}^*$ when flux-weakening control is applied.

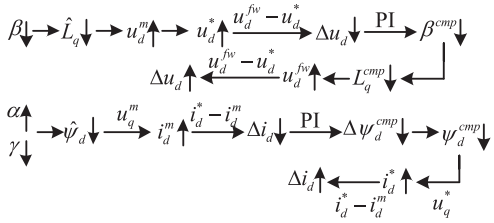

Fig. 9. Signal flow under small signal disturbance condition with $\hat{L}_d$, $\hat{L}_q$, and $\hat{\psi}_f$.

In the command current part of SQCR-VVA flux-weakening control, the initial command currents are given by MTPA limit. Then the correct d-axis command current in flux-weakening region is adjusted by $\Delta i_d^{\mathrm{cmp}}$ from the initial command current. Finally, the q-axis command current in flux-weakening region is calculated by (47).

In the forward feedback voltage calculation part, two groups of feed forward voltages are calculated by the command currents from PART 1. In PART 1, $u_{s,\mathrm{wkfd}}^{\mathrm{fw}}$ is used to obtain $\Delta i_d^{\mathrm{cmp}}$ and $u_{s,\mathrm{mtpa}}^{\mathrm{fw}}$ is used to set Flg_{wk}. When $u_{s,\mathrm{mtpa}}^{\mathrm{fw}} > u_{\max}$, Flg_{wk} is set to 1 and control strategy switches to flux-weakening control; otherwise, Flg_{wk} is set to 0 and control strategy switches to MTPA control.

In the parameters compensation part, two regulators are designed based on the errors of i_d and u_d. The structure of compensation is simple. The compensation variables are β^{cmp} and $\Delta\psi_d^{\mathrm{cmp}}$, and the motor parameters (L_d and ψ_f) in conventional compensation methods are not designed as compensation parameters in proposed method. The final impact of L_q^{cmp} and $\Delta\psi_d^{\mathrm{cmp}}$ on the whole control scheme is the d-axis and q-axis command currents. The compensation method can not influence the stability of SQCR-VVA flux-weakening control method. When the single q-axis current regulator operate normally in SQCR-VVA flux-weakening control, the actual d/q current should be the same as the compensated command value and the accurate torque is implemented.

The signal flow of dual parameter compensation method is shown in Fig. 9. Based on Figs. 8 and 9, the PI regulating process proof is given as follows. The regulating process of β^{cmp} is not affected by the regulating process of α. The initial value of β^{cmp} is 0, and the initial value of L_q^{cmp} is L_q. Firstly, there is a small decrease in $\hat{L}_q$ due to the change of β. When $\hat{L}_q$ decreases, u_d^* will increase because value of u_d^* is negative and u_d^* is controlled to equal to u_d^m. Secondly, the input of PI compensation regulator (Δu_d) decreases, which results in the decrease of β^{cmp}. Affected by β^{cmp}, L_q^{cmp} decreases from L_q. Thirdly, u_d^{fw} will increase because u_d^{fw} is calculated with L_q^{cmp}. The increase of u_d^{fw} will increase the value of Δu_d and the feedback relationship is established. Finally, L_q^{cmp} can be regulated to the value of changed $\hat{L}_q$. The initial value of $\Delta\psi_d^{\mathrm{cmp}}$ is 0, and the initial value of ψ_d^{cmp} is ψ_d. Firstly, there is a small decrease in $\hat{\psi}_d$ due to the change of α and γ. When $\hat{\psi}_d$ decreases, i_d^m will increase because value of i_d^m is negative and u_q^m is affected as fixed value due to the controlled u_d^*. Secondly,

TABLE I
EXPERIMENT SETTINGS AND PARAMETERS OF THE PMSM DRIVE SYSTEM

Parameter	Value	Unit	Parameter	Value	Unit
R_S	2.582	Ω	I_{rate}	5.16	A
L_d	0.025	H	T_{rate}	38	N·m
L_q	0.08	H	N_p	4	-
ψ_f	0.8765	V·s	u_{dc}	540	V
n_{rate}	750	rpm	P_{rate}	3	kW

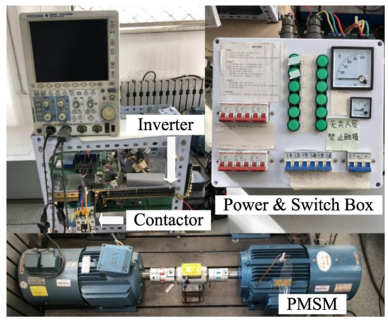

Fig. 10. Experimental platform of 3 kW PMSM drive system.

the input of PI compensation regulator (Δi_d) decreases, which results in the decrease of $\Delta\psi_d^{\rm cmp}$. Affected by $\Delta\psi_d^{\rm cmp}$, $\psi_d^{\rm cmp}$ decreases from ψ_d. Thirdly, i_d^* will increase because u_q^* equals u_q^m. The increase of i_d^* will increase the value of Δi_d and the feedback relationship is established. Finally, $\psi_d^{\rm cmp}$ can be regulated to the value of changed ψ_d^m. Based on (36), T_e^m equals T_e^* with compensated $L_q^{\rm cmp}$ and $\psi_f^{\rm cmp}$. This method is also not designed to compensate α and γ independently.

Although all the three inaccurate PMSM parameters are compensated in Fig. 8, the structure of dual compensation regulators method can be applied for other inaccurate parameters cases. For inaccurate parameter(s) in q-axis voltage calculation, dual compensation regulators is simplified to one compensation regulator base on (24), (28), (33), or (37). When PMSM parameters vary in both d-axis and q-axis voltages calculation, the outputs of PI regulators should be replaced by corresponding compensated parameters, such as $\alpha^{\rm cmp}$ and $\beta^{\rm cmp}$ or $\beta^{\rm cmp}$ and $\gamma^{\rm cmp}$. That is, the proposed method can implement the compensation for different parameters variation cases.

For the sake that d-axis and q-axis current are all controlled by the common field oriented vector control, the impact of inaccurate parameters cannot affect the steady d-axis and q-axis currents response. For nonflux-weakening control structure, the dual parameter compensation regulators based on errors of i_d and u_q cannot implement the compensation goals. Neglecting the voltage of stator resistance and the dynamic performance of single q-axis current regulator, the dual parameters compensation method can operate well in SQCR-VVA flux-weakening control structure.

IV. VERIFICATION OF PROPOSED METHOD

The simulations and experiments are carried out on a 3 kW PMSM platform and the parameters are listed in Table I. The experimental setup is shown in Fig. 10. The PMSM was torque controlled; whereas the load was speed controlled. Legend of the figure for the same y-label is the same.

For all the simulation and experimental figures, $Flg_{\rm par}$ is the sign of parameter change. When $Flg_{\rm par} = 0$, the parameter in control algorithm is the same as the parameter in PMSM model. There was the step change of the parameter in control algorithm at 0.2 s when $Flg_{\rm par}$ switched to 1 in simulation results or 100 in experimental results.

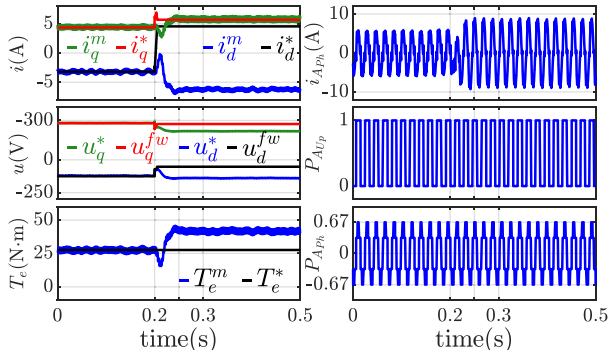

Fig. 11. Simulation results of i_d^m and T_e^m used accurate and inaccurate three parameters without parameters compensation.

A. Simulation Results

1) Impact of Inaccurate Parameters Test: When PMSM parameters are inaccurate, there are 7 basic cases of parameters variation, such as ψ_f variation, L_d variation, L_q variation, ψ_f and L_d variation, L_d and L_q variation, ψ_f and L_q variation, and three parameters variation. Considering that the case of three parameters variation is the complicated and common situation, the impact of inaccurate three parameters on actual d-axis and torque response is shown in Fig. 11. For the left part of figure, the waves in the upper channel are results of i_q^m (Green), i_q^* (Red), i_d^m (Blue), and i_d^* (Black), respectively; the waves in the middle channel are results of u_q^* (Green), $u_q^{\rm fw}$ (Red), u_d^* (Blue), and $u_d^{\rm fw}$ (Black), respectively; the waves in the lower channel are results of T_e^m (Blue) and T_e^* (Black), respectively. For the right part of figure, the waves are A-phase current ($i_{A_{Ph}}$), A-phase upper-leg drive pulse ($P_{A_{Up}}$) and A-phase pulse ($P_{A_{Ph}}$), respectively.

For this test, the PMSM was under SQCR-VVA flux-weakening control with fixed PMSM operation frequency f_s (54 Hz) and fixed command torque T_e^* (27.6 N·m, the maximum torque for $f_s = 54$ Hz operation). The rated frequency $f_{\rm rate}$ is 50 Hz and the rated period is 20 ms. Due to the unchangeable parameters of PMSM model from the Simulink library, the three parameters were changed at 0.2 s. L_d^0 (25 mH), L_q^0 (80 mH) and ψ_f^0 (0.8765 Wb) is the initial values used in SQCR-VVA flux-weakening control, and L_d, L_q, and ψ_f were changed to $0.6L_d^0$, $0.4L_q^0$ and $0.8\psi_f^0$ for this test. When time is in [0, 0.2], the actual d-axis current tracks its command without any d-axis current

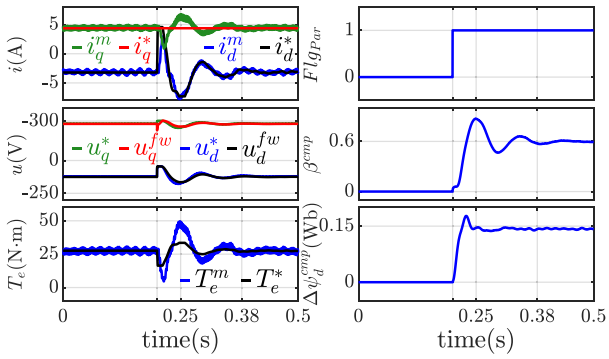

Fig. 12. Simulation results of i_d^m, T_e^m response used accurate and compensated three parameters with parameters compensation.

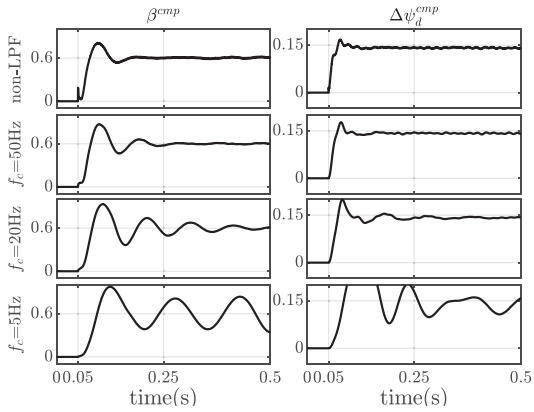

Fig. 13. Simulation results of β^{cmp} and $\Delta\psi_d^{\mathrm{cmp}}$ with different f_c.

related regulator with accurate parameters and actual torque is also accurate compared with its command. After the change of parameters used in SQCR-VVA flux-weakening control (time $>$ 0.2 s), q-axis current is controlled by the single q-axis current and the dynamic regulation period is less than 40 ms under the low switching frequency (54 Hz for the square-wave modulation). For the steady results, actual d-axis cannot track its command and the command current working point, which results in the error between the command and actual torques.

2) Dual Parameters Compensation Test: In order to improve the accuracy of output torque, the dual parameters compensation algorithm is applied after the change of PMSM parameters. The compensated parameters results are shown in Fig. 12. For the right part of figure, the waves are replaced by flag of changed parameters (Flg_{par}), q-axis inductance compensation coefficient (β^{cmp}) and d-axis flux compensation value ($\Delta\psi_d^{\mathrm{cmp}}$), respectively.

For this test, the operation condition is the same as the condition in "Impact of inaccurate parameters test". L_q was step changed to 32 mH ($0.4L_q^0$), but β^{cmp} was regulated by the dual PI regulators to 0.6, which shows the implementation of compensation for inaccurate q-axis inductance. L_d was changed to 15 mH ($0.6L_d^0$) and ψ_f was changed to 0.7012 Wb ($0.8\psi_f^0$), which resulted that ψ_d was reduced by 0.143153 Wb ($0.2\psi_f^0$ + $0.4L_d^0 \times i_d^*$, $i_d^* = -3.217$). As shown in the Fig. 12, $\Delta\psi_d^{\mathrm{cmp}}$ is also compensated at the same time. Applied the compensation control, the average of steady command and actual torques between 0.338 and 0.35 s are regulated to 27.43 and 27.16 N·m, respectively. The error ratio of command and actual torques are -0.616% and -1.59%, respectively. The compensated torque results show the quite good performance on the improvement of torque accuracy.

3) Impact of Low-Pass Filter With Different Cut-Off Frequencies Test: When β^{cmp} and $\Delta\psi_d^{\mathrm{cmp}}$ have been regulated, the compensation work does not finish and they should be used by PART 1 and 2 in Fig. 8. However, the fluctuation of u_d^*, u_d^{fw}, β^{cmp} and $\Delta\psi_d^{\mathrm{cmp}}$ can affect the compensation performance. Low-pass filters (LPFs) for input of β^{cmp} PI regulator, β^{cmp} and $\Delta\psi_d^{\mathrm{cmp}}$ can be applied to reduce the fluctuation. The impact of low-pass filter with different cut-off frequencies is shown in Fig. 13. For the left part of figure, the waves are results of (β^{cmp}); for the right part of figure, the waves are results of ($\Delta\psi_d^{\mathrm{cmp}}$). In the top channel, LPFs are not applied. f_c is the cut-off frequency of the LPFs, which is 50, 20, or 5 Hz for the second, third and bottom channels, respectively.

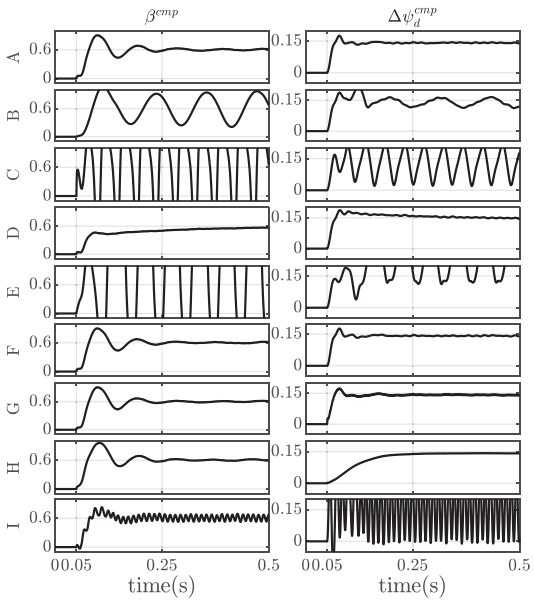

Fig. 14. Simulation results of β^{cmp} and $\Delta\psi_d^{\mathrm{cmp}}$ with different $K_p^{u_d}$, $K_i^{u_d}$, $K_p^{i_d}$ and $K_i^{i_d}$.

As shown in Fig. 13, LPFs contribute to the reduction of high frequency fluctuations. However, the lower cut-off frequency of LPFs is, the worse dynamic performance of dual parameter compensation PI regulators are. If the fluctuation of β^{cmp}, $\Delta\psi_d^{\mathrm{cmp}}$ and T_e^* is acceptable, the proposed method can work well with no LPF. When LPFs are applied, cut-off frequency around f_{rate} is recommended.

4) Impact of of Compensation PI Regulators With Different K_p and K_i Test: For the sake that PI regulators are applied in the dual parameters compensation method, the performance is affected by different proportional and integral coefficients. The impact of $K_p^{u_d}$, $K_i^{u_d}$, $K_p^{i_d}$, and $K_i^{i_d}$ is shown in Fig. 14. The specific values of dual parameters compensation regulators are

TABLE II
VALUES OF $K_p^{u_d}$, $K_i^{u_d}$, $K_p^{i_d}$, AND $K_i^{i_d}$

Case	$K_p^{u_d}$	$K_i^{u_d}$	$K_p^{i_d}$	$K_i^{i_d}$
A	$\mathbf{1.0}K_{p0}^{u_d}$	$\mathbf{1.0}K_{i0}^{u_d}$	$\mathbf{1.0}K_{p0}^{i_d}$	$\mathbf{1.0}K_{i0}^{i_d}$
B	$\mathbf{0.1}K_{p0}^{u_d}$	$1.0K_{i0}^{u_d}$	$1.0K_{p0}^{i_d}$	$1.0K_{i0}^{i_d}$
C	$\mathbf{10}K_{p0}^{u_d}$	$1.0K_{i0}^{u_d}$	$1.0K_{p0}^{i_d}$	$1.0K_{i0}^{i_d}$
D	$1.0K_{p0}^{u_d}$	$\mathbf{0.1}K_{i0}^{u_d}$	$1.0K_{p0}^{i_d}$	$1.0K_{i0}^{i_d}$
E	$1.0K_{p0}^{u_d}$	$\mathbf{10}K_{i0}^{u_d}$	$1.0K_{p0}^{i_d}$	$1.0K_{i0}^{i_d}$
F	$1.0K_{p0}^{u_d}$	$1.0K_{i0}^{u_d}$	$\mathbf{0.1}K_{p0}^{i_d}$	$1.0K_{i0}^{i_d}$
G	$1.0K_{p0}^{u_d}$	$1.0K_{i0}^{u_d}$	$\mathbf{10}K_{p0}^{i_d}$	$1.0K_{i0}^{i_d}$
H	$1.0K_{p0}^{u_d}$	$1.0K_{i0}^{u_d}$	$1.0K_{p0}^{i_d}$	$\mathbf{0.1}K_{i0}^{i_d}$
I	$1.0K_{p0}^{u_d}$	$1.0K_{i0}^{u_d}$	$1.0K_{p0}^{i_d}$	$\mathbf{10}K_{i0}^{i_d}$

listed in Table II. The basic values of $K_p^{u_d}$, $K_i^{u_d}$, $K_p^{i_d}$, and $K_i^{i_d}$ are $K_{p0}^{u_d}$ (0.0125), $K_{i0}^{u_d}$ (0.875), $K_{p0}^{i_d}$ (0.01), and $K_{i0}^{i_d}$ (0.0006), respectively.

As shown in Fig. 14, the larger values for proportional or integral coefficients can cause the oscillation of β^{cmp} and $\Delta\psi_d^{\mathrm{cmp}}$, such as cases of C, E, and I. The smaller values for proportional or integral coefficients cannot cause the oscillation of β^{cmp} and $\Delta\psi_d^{\mathrm{cmp}}$, such as cases of D, F, and H. However, there are two exceptional cases (B and G). For case B, the smaller proportional coefficient results in the oscillating dynamic performance of PI regulator based on u_d. PI regulator based on u_d is the first regulating loop of the whole compensation control and its performance affects PI regulator based on i_d. The interaction between the two PI regulators results in worse oscillating performance. The non-oscillation performance of PI regulator based on u_d should be guaranteed. For case G, the larger proportional coefficient cannot result in a bigger oscillation because PI regulator based on i_d is the second regulating loop of the whole compensation control and its performance does not affect by PI regulator based on u_d seriously. If only PI regulator based on u_d is studied, the dynamic regulating period can be adjusted to around 40 ms (two rated periods). The existed parameters compensation, estimation or identification methods are seldom applied in low switching frequency operation and their dynamic regulating period in high switching frequency is around 5 to 50 ms. The proposed compensation method is designed using the feature that d-axis is not controlled in original SQCR-VVA flux-weakening control structure. The actual q-axis current should be tracked perfectly. However, the dynamic regulating period of the single q-axis current regulator is around 40 ms. The total dynamic regulating period of dual parameters compensation PI regulators is surely more than 40 ms, but the period can be less than 120 ms with suitable proportional or integral coefficients in the low switching frequency (around 50 Hz) operation.

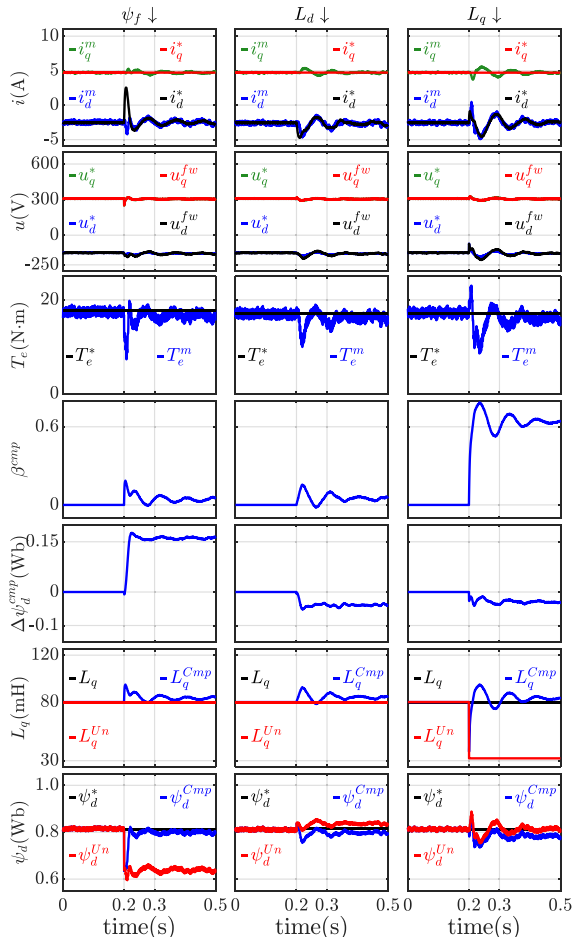

Fig. 15. Experimental results of single step-down changed parameter.

B. Experimental Results

The propose method is also tested by the ground tests base on the 3-kW PMSM platform. According to the results and analysis of Fig. 13, the cut-off frequencies of LPFs are given by the same value, 50 Hz. Moreover, according to the the results and analysis of Fig. 14, the proportional or integral coefficients of dual parameters compensation regulators are given by 0.0125 ($K_p^{u_d}$), 0.875 ($K_i^{u_d}$), 0.01 ($K_p^{i_d}$), and 0.0006 ($K_i^{i_d}$), respectively. The stator frequency of PMSM was also 54 Hz. Under these settings, 14 different parameters variation cases were tested and the detailed experimental results were shown in Figs. 15–19.

In each experimental figure, 7 types of variables are presented in 7 rows, respectively. From top row to button row, the variables are currents (i_q^*, i_q^m, i_d^* and i_d^m), voltages (u_q^*, u_q^{fw}, u_d^* and u_d^{fw}), torques (T_e^* and T_e^m), compensation of β (β^{cmp}), compensation of ψ_d ($\Delta\psi_d^{\mathrm{cmp}}$), q-axis inductances (fixed value L_q, uncompensated value L_q^{Un} and compensated value L_q^{cmp}), and d-axis fluxes (command value ψ_d^*, uncompensated value ψ_d^{Un} and compensated value ψ_d^{cmp}), respectively. The time axis is divided into three periods: period one (0-0.2 s), period two (0.2–0.3 s), and period three (0.3–0.5 s). In period one, the parameters were accurate. At 0.2 s, the parameters were step changed. In period

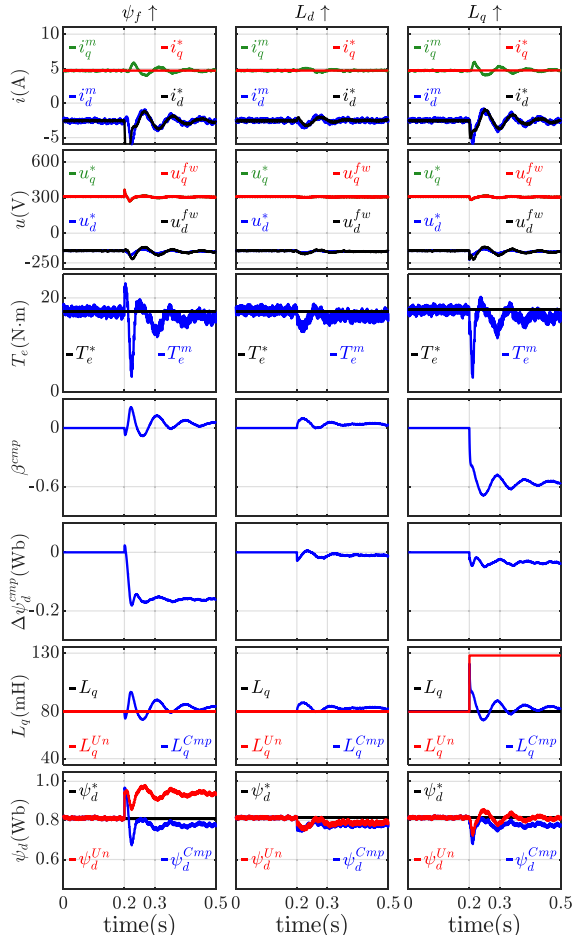

Fig. 16. Experimental results of single step-up changed parameter.

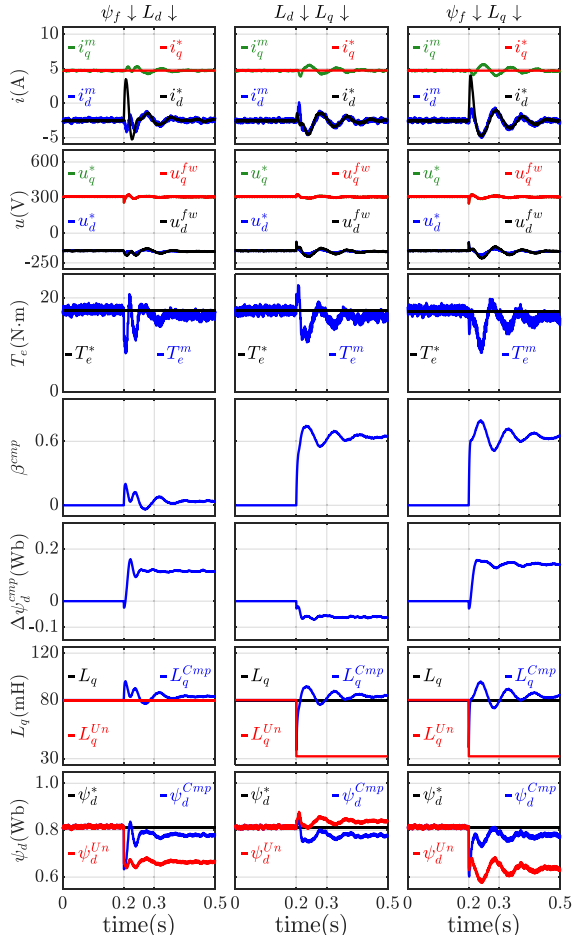

Fig. 17. Experimental results of two step-down changed parameters.

two and three, the proposed method operated to suppress the impact of inaccurate parameters and compensate torque. For light impact, performance of compensation was achieved in period two; for serious impact, performance of compensation was achieved in period three.

The experimental results for single inaccurate parameter compensation are shown in Figs. 15 and 16. In Fig. 15, ψ_f, L_d and L_q were step changed to $0.8\psi_f^0$, $0.6L_d^0$, and $0.4L_q^0$ at 0.2 s for the left, middle and right parts of the figure, respectively. It can be known from the waves of β^{cmp}, $\Delta\psi_d^{\mathrm{cmp}}$, L_q, and ψ_d that dual parameters compensation control can be suitable for single inaccurate parameter compensation. For changed ψ_f or L_d case, the final value of β^{cmp} is not fluctuating around zero with the fixed L_q. The average value of β^{cmp} between 0.38 and 0.5 s is 0.0423, which means there is a less than 5% error between the compensated q-axis inductance and the original q-axis inductance form Table I. For changed L_q case,the final value of $\Delta\psi_d^{\mathrm{cmp}}$ is not fluctuating around zero with the fixed L_d and ψ_f. The average value of $\Delta\psi_d^{\mathrm{cmp}}$ between 0.38 and 0.5 s is -0.0345 Wb, which means there is a maximum -3.93% error from ψ_f or a maximum 53% error from L_d. The result of $\Delta\psi_d^{\mathrm{cmp}}$ from change L_q case illustrate the feature of proposed method that the compensation of impact of inaccurate L_d or ψ_f cannot be implemented and the compensation of impact of both inaccurate L_d and ψ_f can be achieved. Additionally, the impact of error in L_d and ψ_f of experimental platform can be equivalent to -3.93% error from ψ_f, which means this error is also very small. Based on the analysis in Section III and subsection IV-A, accurate torque is achieved when the d-axis and q-axis currents are controlled to their command values, which is shown in channel 3 with legends of command torque T_e^* and actual torque T_e^m.

In Fig. 16, ψ_f, L_d and L_q were step changed to $1.2\psi_f^0$, $1.4L_d^0$, and $1.6L_q^0$ at 0.2 s for the left, middle and right parts of the figure, respectively. Similar to Fig. 15, Fig. 16 shows that single inaccurate parameter compensation was achieved and output torque tracked its command value after parameter was step-up changed.

The experimental results for two inaccurate parameters compensation are shown in Figs. 17 and 18. In Fig. 17, ψ_f, L_d and L_q were step changed to $0.8\psi_f^0$ and $0.6L_d^0$, $0.6L_d^0$ and $0.4L_q^0$, and $0.8\psi_f^0$ and $0.4L_q^0$, at 0.2 s for the left, middle and right parts of the figure, respectively. In Fig. 18, ψ_f, L_d and L_q were step changed to $1.2\psi_f^0$ and $1.4L_d^0$, $1.4L_d^0$ and $1.6L_q^0$, and $1.2\psi_f^0$ and $1.6L_q^0$, at 0.2 s for the left, middle and right parts of the figure, respectively. The results of β^{cmp} and $\Delta\psi_d^{\mathrm{cmp}}$ present

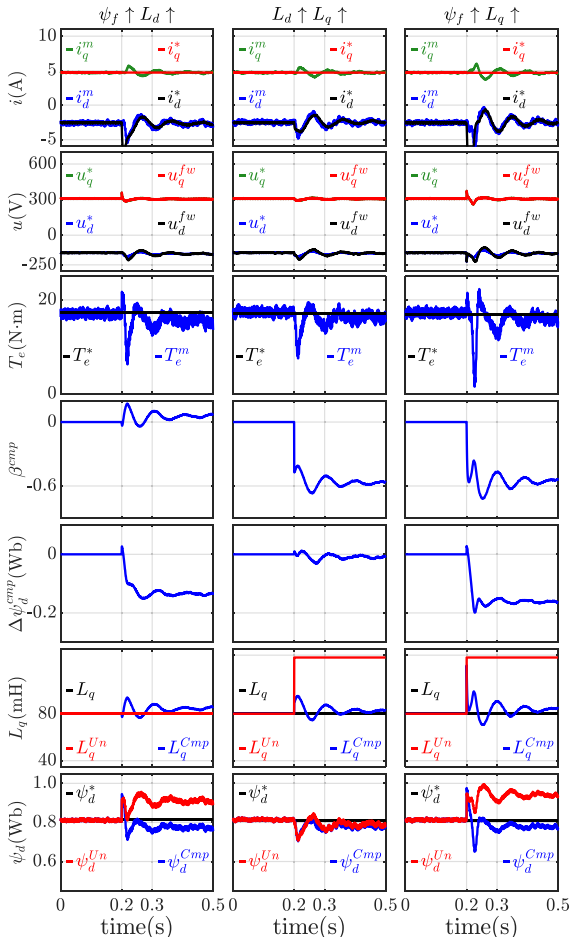

Fig. 18. Experimental results of two step-up changed parameters.

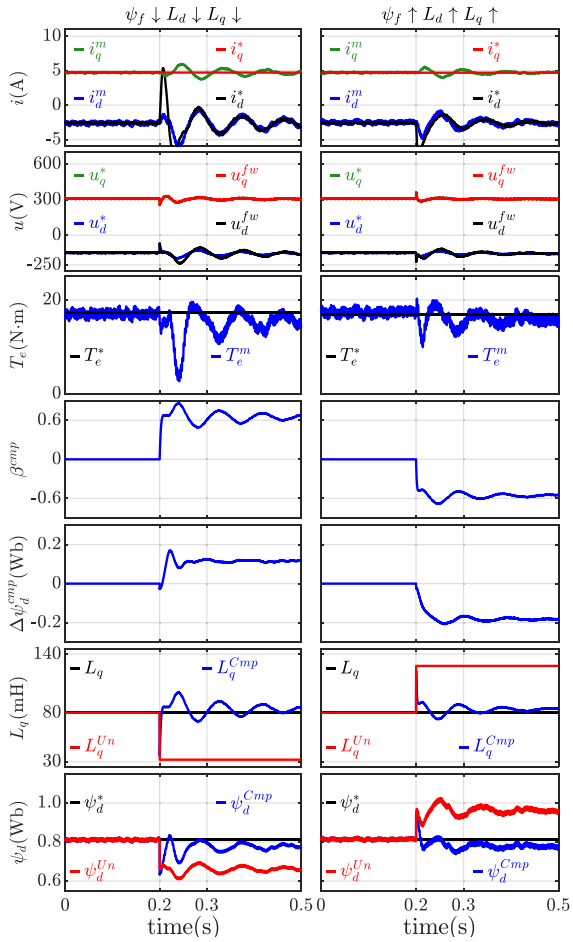

Fig. 19. Experimental results for three inaccurate parameters compensation.

the regulation process of elimination of the errors in d-axis current and d-axis voltage, respectively. Similar to Figs. 15 and 16, the blue waveforms of L_q^{Cmp} track the fixed L_q, but there is still a very small steady error which is less than 5%. For the compensation results of ψ_d, no matter how the inaccurate parameters condition is, ψ_d^{cmp} is controlled to almost the same value. It can be known from the waves of β^{cmp}, $\Delta\psi_d^{\mathrm{cmp}}$, L_q, and ψ_d that dual parameters compensation control is also suitable for two inaccurate parameters compensation. When β^{cmp} and $\Delta\psi_d^{\mathrm{cmp}}$ were regulated to the right compensation values, output torque was controlled within 5% torque error.

In three inaccurate parameters compensation tests, the changes of parameters in step decrease and step increase cases are applied and corresponding experimental results are shown in Fig. 19. For the step decrease case in the left part of the figure, ψ_f, L_d, and L_q were step changed to $0.8\psi_f^0$, $0.6L_d^0$, and $0.4L_q^0$ at the same time of 0.2 s; for the step increase case in the right part of the figure, ψ_f, L_d, and L_q were step changed to $1.2\psi_f^0$, $1.4L_d^0$, and $1.6L_q^0$ at the same time of 0.2 s. Compared with simulation tests, the dynamic regulating periods of experimental tests are longer. The main reason is that the there exists the fluctuation of f_s after parameters were changed. Although the speed was controlled by an induction motor, there existed the dynamic regulating period for the induction motor and the performance of speed control is not perfect, which results in the fluctuation of speed. Then the fluctuation of speed results in the slow dynamic regulating of single q-axis current regulator in SQCR-VVA flux-weakening control and finally affects the performance of proposed method. Compared with the results shown in Figs. 15–18, β^{cmp} and $\Delta\psi_d^{\mathrm{Cmp}}$ are still under control with the most serious variation of parameters, and the steady waves of T_e^m show the quite good performance of L_q and ψ_d compensation control through waves of β^{cmp} and $\Delta\psi_d^{\mathrm{cmp}}$. Although the actual variation of parameters of d-axis inductance, q-axis inductance and permanent magnet flux may be not the same as the tested condition, the proposed compensation method can deal with the impact of complex inaccurate parameters conditions.

V. Conclusion

The accuracy of torque is the key in rail transit system, especially in flux-weakening region. When SQCR-VVA flux-weakening control method is applied, the impact of inaccurate PMSM parameters results in the errors of i_d, u_d, and T_e. Based on the d-axis current error response with the variation of parameters, d-axis feed-forward voltage compensation and d-axis flux compensation are applied to the proposed compensation

method. Compared with the existing methods, the structure of proposed method is simpler. The impact of inaccurate L_d, L_q, ψ_f can be equivalent to the impact of L_q and ψ_d, which are compensated by β^{cmp} and $\Delta\psi_d^{\mathrm{cmp}}$ at the same time. The feasibility and effectiveness of the proposed method has been verified by both computer simulation and experimental results.

REFERENCES

[1] Y. Chen, W. Chen, J. Zhou, Y. Fang, and Y. Yao, "Multi-field coupled analysis of a permanent magnet synchronous motor: Application to high speed rail traction," in *Proc. 11th Int. Conf. Ecological Veh. Renewable Energies*, 2016, pp. 1–6.

[2] C. Calleja, A. López-de-Heredia, H. Gaztañaga, L. Aldasoro, and T. Nieva, "Validation of a modified direct-self-control strategy for PMSM in railway-traction applications," *IEEE Trans. Ind. Electron.*, vol. 63, no. 8, pp. 5143–5155, Aug. 2016.

[3] H. Douglas, F. Schmid, C. Roberts, and S. Hillmansen, "Evaluation of permanent magnet motor energy saving technology for different types of railways," in *Proc. IEEE Int. Conf. Intell. Rail Transp.*, 2016, pp. 123–129.

[4] E. Armando, R. I. Bojoi, P. Guglielmi, G. Pellegrino, and M. Pastorelli, "Experimental identification of the magnetic model of synchronous machines," *IEEE Trans. Ind. Appl.*, vol. 49, no. 5, pp. 2116–2125, Sep./Oct. 2013.

[5] G. Pellegrino, B. Boazzo, and T. M. Jahns, "Magnetic model self-identification for PM synchronous machine drives," *IEEE Trans. Ind. Appl.*, vol. 51, no. 3, pp. 2246–2254, May/Jun. 2015.

[6] K. Liu, J. Feng, S. Guo, L. Xiao, and Z. Q. Zhu, "Identification of flux linkage map of permanent magnet synchronous machines under uncertain circuit resistance and inverter nonlinearity," *IEEE Trans. Ind. Informat.*, vol. 14, no. 2, pp. 556–568, Feb. 2018.

[7] S. J. Underwood and I. Husain, "Online parameter estimation and adaptive control of permanent-magnet synchronous machines," *IEEE Trans. Ind. Electron.*, vol. 57, no. 7, pp. 2435–2443, Jul. 2010.

[8] S. Nalakath, M. Preindl, and A. Emadi, "Online multi-parameter estimation of interior permanent magnet motor drives with finite control set model predictive control," *IET Elect. Power Appl.*, vol. 11, no. 5, pp. 944–951, 2017.

[9] Q. Liu and K. Hameyer, "A fast online full parameter estimation of a PMSM with sinusoidal signal injection," in *Proc. IEEE Energy Convers. Congr. Expo.*, Sep. 2015, pp. 4091–4096.

[10] K. Liu and Z. Q. Zhu, "Online estimation of the rotor flux linkage and voltage-source inverter nonlinearity in permanent magnet synchronous machine drives," *IEEE Trans. Power Electron.*, vol. 29, no. 1, pp. 418–427, Jan. 2014.

[11] G. Feng, C. Lai, K. Mukherjee, and N. C. Kar, "Online PMSM magnet flux-linkage estimation for rotor magnet condition monitoring using measured speed harmonics," *IEEE Trans. Ind. Appl.*, vol. 53, no. 3, pp. 2786–2794, May/Jun. 2017.

[12] W. Deng, C. Xia, Y. Yan, Q. Geng, and T. Shi, "Online multiparameter identification of surface-mounted PMSM considering inverter disturbance voltage," *IEEE Trans. Energy Convers.*, vol. 32, no. 1, pp. 202–212, Mar. 2017.

[13] K. Liu and Z. Q. Zhu, "Position offset-based parameter estimation for permanent magnet synchronous machines under variable speed control," *IEEE Trans. Power Electron.*, vol. 30, no. 6, pp. 3438–3446, Jun. 2015.

[14] A. Quntao and S. Li, "On-line parameter identification for vector controlled PMSM drives using adaptive algorithm," in *Proc. IEEE Veh. Power Propulsion Conf.*, Sep. 2008, vol. 1, no. 1, pp. 1–6.

[15] P. Caldori, A. Guagnano, V. G. Monopoli, and F. Cupertino, "Inductance measurement methods for position estimation in permanent magnet synchronous motors," in *Proc. IEEE Int. Conf. Elect. Mach.*, 2016, pp. 1078–1084.

[16] O. C. Kivanc and S. B. Ozturk, "Sensorless PMSM drive based on stator feedforward voltage estimation improved with MRAS multiparameter estimation," *IEEE/ASME Trans. Mechatron.*, vol. 23, no. 3, pp. 1326–1337, Jun. 2018.

[17] S. Cho, W. Shin, J. Park, and W. Kim, "A torque compensation control scheme of PMSM considering wide variation of permanent magnet temperature," *IEEE Trans. Magn.*, vol. 55, no. 2, Feb. 2019, Art. no. 8200105.

[18] T. Boileau, B. Nahid, and F. Meibody, "Online identification of PMSM parameters: Parameter identifiability and estimator comparative study," *IEEE Trans. Ind. Appl.*, vol. 47, no. 4, pp. 1944–1957, Jul./Aug. 2011.

[19] T. Boileau, B. Nahid, and F. Meibody, "On-line identification of PMSM parameters: Model-reference vs EKF," in *Proc. IEEE Ind. Appl. Soc. Annu. Meeting*, Oct. 2008, pp. 1–8.

[20] X. Fang, T. Wang, Z. Yang, and F. Lin, "Permanent magnet synchronous traction motor torque close-loop control based on stator flux observation for urban rail train," in *Proc. Asian Conf. Energy, Power Transp. Electrific.*, 2016, pp. 1–6.

[21] S. Wu, J. Zhang, H. Chen, and P. Wang, "An adaptive position observer with parameters estimation for surface-mount permanent magnet synchronous motor," in *Proc. Int. Conf. Intell. Connected Veh.*, 2016, pp. 1–5.

[22] Z. Xiaoguang and H. Benshuai, "A flux observer for a direct torque controlled permanent-magnet synchronous machine control system," in *Proc. Int. Power Electron. Motion Control Conf.*, 2016, pp. 1373–1377.

[23] Z. Zhang, C. Wang, M. Zhou, and X. You, "Flux-weakening in PMSM drives: Analysis of voltage angle control and the single current controller design," *IEEE J. Emerg. Sel. Topics Power Electron.*, vol. 7, no. 1, pp. 437–445, Mar. 2019.

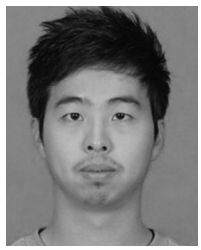

Zisui Zhang (Member, IEEE) was born in Henan, China, in 1990. He received the B.S. and Ph.D. degrees in electrical engineering in 2013 and 2019, respectively, from Beijing Jiaotong University, Beijing, China, where he is currently working toward the Ph.D. degree in electrical engineering.

His current research interests include PMSM control.

Chenchen Wang (Member, IEEE) was born in Anhui, China, in 1981. He received the B.S. and Ph.D. degrees in electrical engineering from Tsinghua University, Beijing, China, in 2003 and 2008, respectively.

He is presently working as an Associate Professor in the School of Electrical Engineering, Beijing Jiaotong University, Beijing, China. His current research interests include electric drive and multilevel converters.

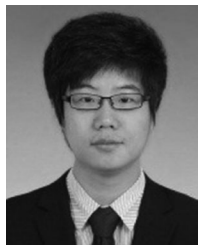

Minglei Zhou (Member, IEEE) was born in Shandong, China, on September 16, 1985. He received the bachelor's and Ph.D. degrees from the School of Electrical Engineering, Beijing Jiaotong University (BJTU), in 2007 and 2013 respectively.

He is presently working as an Associate Professor in the School of Electrical Engineering BJTU. His research interests include the control of electrical machines and high-power traction driving systems.

Xiaojie You was born in Fujian, China, in 1964. He received his M.S. degree in electrical engineering from the China Agricultural University, Beijing, China, in 1989, and the Ph.D. degree from the Czech Technical University, Prague, Czech Republic, in 2001.

He is presently working as a Professor and also the Director of Power Electronic Research Institute in the School of Electrical Engineering, Beijing Jiaotong University, Beijing, China. His current research interests include ac drive electric locomotive control, switching power control, active power filters and power quality control.